Behaviour of macroscopic rigid spheres in Poiseuille flow

Part 2. Experimental results and interpretation

By G. SEGRÉ† AND A. SILBERBERG
Weizmann Institute of Science, Rehovoth, Israel

(Received 6 November 1961 and in revised form 16 March 1962)

It is shown that a rigid sphere transported along in Poiseuille flow through a tube is subject to radial forces which tend to carry it to a certain equilibrium position at about 0·6 tube radii from the axis, irrespective of the radial position at which the sphere first entered the tube. It is further shown that the trajectories of the particles are portions of one master trajectory and that the origin of the forces causing the radial displacements is in the inertia of the moving fluid. An analysis of the parameters determining the behaviour is presented and a phenomenological description valid at low Reynolds numbers is arrived at in terms of appropriate reduced variables. These phenomena have already been described in a preliminary note (Segré & Silberberg 1961). The present more complete analysis confirms the conclusions, but it appears that the dependence of the effects on the particle radius go with the third and not the fourth power as was then reported.

It is also shown that the description of the phenomena becomes more complicated at tube Reynolds numbers above about 30.

1. Introduction

The occurrence of a 'tubular pinch' effect in laminar flow of suspensions of spheres through a tube has been reported in a preliminary note (Segré & Silberberg 1961). From this it appears that particles are subject to radial displacements, outwards from the centre of the tube and inwards from its wall. There exists an equilibrium radial position at about 0·6 tube radii from the axis to which the particles tend. The origin of these effects lies in the inertia of the fluid.

Radial displacements of spherical particles in streaming suspensions have been suspected in the past in view of certain deviations from the ideal in the flow behaviour of such systems. In particular, viscosity experiments tend to give results which, depending on flow conditions, are lower than those calculated from the Einstein equation. Some observations of this kind have been termed σ-phenomena by Scott-Blair who recently (1958) gave a rather extensive review of anomalous viscosity behaviour of suspensions.

More direct studies of particle displacements are also reported and studies of concentration changes go back to Poiseuille (1836) who in blood flow noticed a corpuscle-free region near the walls of the capillary. Perhaps the most elegant

† On leave from Cartiera Vita Mayer and Co., Milan, Italy.

observations of uneven distribution of erythrocytes in flowing blood are those of Taylor (1955). Taylor scanned the cross-section of the flow tube and observed a region of low absorbancy not only near the wall but also near the centre of the tube, provided the velocity of flow was large enough. These results which closely confirm ours were however given a different explanation by the author. In the extensive review of the rheology of blood by Frey-Wyssling (1952, ch. VI), evidence is presented for corpuscle displacements mainly tending to show that the particles are driven towards the centre. The possibility that some dispersing action opposes this tendency is however hinted at mainly because the experimental results are not consistent with a tight packing of corpuscles in the centre. This point is also made in a discussion by Bayliss (1960, p. 29) on anomalous blood viscosity.

Among studies with other systems in which particle displacements in flowing suspensions were observed or inferred one may mention in particular those of Tollert (1954) and Maude & Whitmore (1956).

The more direct approach to the problem by way of observation of single particle motion is rather difficult and such studies are relatively few. The case most directly comparable with our experiments is to the best of our knowledge the investigation of Vejlens (1938) who used a square-cross-section flow tube with glass windows in which the trajectory of a rigid sphere released from near the wall could be observed photographically. He found that the particle moved away from the wall and that this effect increased rapidly with particle size. His results compare well with ours if we make allowance for the different flow conditions.

Recently Goldsmith & Mason (1961) reported experiments on rigid spheres in Poiseuille flow where no sideward displacements were observed. Unfortunately they conducted their studies under conditions where no measurable effects are to be expected according to our results.

While many authors mention the possibility of radial forces and advance qualitative reasons for their existence there are few thoroughgoing investigations. Moreover, all the arguments advanced are in support of a force directed radially inwards.

A fundamental investigation into the nature of the problem is due to Simha (1936) who solved the case of a rigid sphere carried in an unbounded Poiseuille field of flow. His solution is based on the linearized Navier–Stokes equations, i.e. he deals only with creeping motion, and shows that under these circumstances there is no radially directed motion. It is clear therefore that the cause for sideward particle displacements must be sought either in the neglected inertia terms of the equations of motion, or in the presence of the rigid walls, or in both.

The case of a particle moving alongside a rigid wall was discussed for different conditions of flow by several authors (Lorentz 1907, p. 23; Vand 1948; Happel & Brenner 1958). From these results, which all refer to creeping motion, it appears, however, that despite the presence of the wall no sideward force acts on the particle.

The first formal derivation of an inwardly directed lateral force based on inertia effects may be found in the use of the Kutta–Joukowsky formula made by

Tollert (1954) for particles sedimenting in the presence of walls. His treatment thus attributes the phenomenon to the Magnus effect. A rigorous consideration of the effect of inertial forces is due to Saffman (1956) who however treated only an unbounded Poiseuille field. The force found by Saffman is also directed inwards. The case of a spinning sphere dragged through a viscous fluid at rest is treated by Rubinow & Keller (1961) using Stokes and Oseen expansions of the complete equations of motion. Also in this case a transverse force whose leading term is functionally identical with and in the same sense as the Magnus force is deduced.

Summarizing it appears that the effect found by us can account for the experimental observations that have been made in various cases, and that the radial displacements are due to the inertia of the fluid. While purely inward motion has been made plausible by the above considerations no satisfactory analysis to explain the outward displacements from the centre has yet been advanced.

2. Experiment

An account of the apparatus and method has been given in Part 1 of this paper (Segré & Silberberg 1962). The system investigated consisted of suspensions of polymethylmethacrylate spheres with a narrow distribution of diameters in media composed of mixtures of glycerol, 1,3-butanediol and water adjusted to match the density of the spheres, $\rho_{34^\circ} = 1{\cdot}178\,\mathrm{g/cm^3}$. The mean particle diameters were $2a = 0{\cdot}32$, $0{\cdot}80$, $1{\cdot}21$ and $1{\cdot}71$ mm. The viscosity of the fluid resulting from mixtures in different proportions of the components varied between 17 and 410 cP. The overall particle concentrations C_0 ranged from 0·33 to 4 particles per $\mathrm{cm^3}$.

A fixed volume (660 $\mathrm{cm^3}$) of the suspension was made to flow through a vertical tube of inner radius $R = 5{\cdot}6$ mm and the concentration at various points analysed by scanning the cross-section of the tube with two mutually perpendicular light beams.† The interruptions of the light beams by particles passing through them were transduced photoelectrically and these pulses counted and analysed as discussed in Part 1. From this analysis the number of particle passages N_h through the narrow common crossing-over region of the beams was calculated. The concentration distribution $C(r, z)$, where r is the radial position and z is the co-ordinate along the tube axis, is then determined from N_h on the assumption that the particle velocity in the z-direction coincides with the velocity of the liquid in the Poiseuille field

$$V = 2V_m[1 - (r/R)^2].$$

The distance l of the scanning section from the mouth of the tube could be varied from 6 to 120 cm and the mean velocity of flow V_m was adjustable within the range 5 to 90 cm/sec.

Experiments were performed in series, each series representing a given suspension (given η, a, ρ and C_0) made to flow under given conditions (given V_m) and observed at a given distance from the mouth of the tube (given l). At least twenty measurements were made at each radial setting r and the average used to compute the N_h and C distributions for the series.

† In Segré & Silberberg (1961) the tube diameter was through an oversight given as 11·6 mm.

3. Results

Table 1 gives a summary of the conditions under which the various series of experiments were performed. The parameters listed are $2a$, C_0, η, l, V_m and the Reynolds number for the tube

$$\mathrm{Re} = \rho V_m 2R/\eta.$$

The further quantities listed in the table will be explained later.

Figures 1 to 3 show the N_h, and in most cases the C, distributions in terms of tube radial position r for some of the series mentioned in the table. Figure 4 shows the results for N_h plotted against r^2 for those series where it was desirable to test whether N_h followed a parabolic law.

4. Discussion of results

(*a*) *Studies of flow near tube inlet*

As already pointed out we are assuming that the velocity profile in the flow tube is given by a parabolic law and that the velocity of the particles in the z-direction coincides with this velocity $V(r) = 2V_m[1-(r/R)^2]$ of the undisturbed liquid. Near the mouth of the tube, before any major sideward displacement of particles could have taken place, the concentration of particles should still be uniform and the 'hits' number N_h, which is proportional to CV, should thus be distributed parabolically across the tube. (For a detailed discussion of the functional relation between N_h and CV reference should be made to Part 1.) Under suitable conditions therefore, a plot of N_h against r^2 should be linear with an intercept on the r^2 axis given by R^2. Such plots are shown in figure 4 and attention is drawn particularly to series S. 7, S. 9 and S. 38 by which the validity of the above assumptions may be regarded as established for the cross-sections in question.

Further down the tube where large deviations from the parabolic distribution of N_h are measured it is not possible *a priori* to decide what part, if any, is due to changes in velocity. In view of the low Reynolds numbers employed (see table 1) and the fact that a laminar state was reached shortly below the tube mouth it is reasonable to assume, as we have done, that this laminar solution is stable right through the tube. Some more direct evidence for this will appear later.

The other diagrams in figure 4 corresponding to series S. 13, S. 15, S. 17, S. 39 and S. 40 refer to observations at tube cross-sections effectively farther away from the mouth (i.e. at larger L-values, see later discussion) than the series mentioned above and deviations from the parabolic law may be already noticed above the experimental scatter.

It is clear that fluid entering the mouth of the tube from the stirred storage container will not immediately settle into the laminar parabolic flow pattern. Even under the most ideal conditions a certain 'inlet length' Λ must be allowed for before the profile has been established. Following Smith (1960) we put $\Lambda = 0{\cdot}13R\,\mathrm{Re}$ and find the values listed in table 1. In most cases Λ is only a small fraction of the length l and we have made no allowance for it in our calculations. While the real transition region will probably exceed the ideal Λ in our experiments, the error remains negligible in comparison with other errors in cases of Reynolds numbers less than 30.

Series	$2a$ (mm)	C_0 (part./cm^3)	η (poise)	l (cm)	V_m† (cm/sec)	Re	Λ‡ (cm)	Δx (mm)	r_{lim} (mm)	$\bar{r}$ (mm)	Δr (mm)	C_{eff}§ (part./cm^3)	$\frac{C(0,l)}{C_{eff}}$	L_3	L_4
1	0·32	3	0·17	31	22·3	173	12·6	—	—	—	—	—	—	0·11	0·003
2	0·32	3	0·17	120	22·3	173	12·6	—	—	—	—	—	—	0·43	0·012
3	0·32	3	0·17	31	33·5	260	19	—	—	—	—	—	—	0·17	0·005
4	0·32	3	0·17	120	33·5	260	19	—	—	—	—	—	—	0·65	0·019
5	0·32	3	0·17	31	67·0	520	38	—	—	—	—	—	—	0·34	0·009
6	0·32	3	0·17	120	67·0	520	38	—	—	—	—	—	—	1·30	0·037
7	0·80	1	3·92	31	11·22	3·7	0·27	1·38	5·2	2·60	1·51	0·86	1·00	0·037	0·0026
8	0·80	1	3·92	120	48·2	16·2	1·18	1·50	4·10	2·70	1·21	0·81	0·61	0·63	0·044
9	0·80	2	4·30	31	11·06	3·4	0·25	1·31	5·2	2·60	1·51	1·78	1·00	0·034	0·0024
10	0·80	2	4·30	120	47·8	14·7	1·07	1·50 1·25	4·10 4·20	2·83 2·85	1·10 1·16	1·39 1·95	0·61 0·61	0·57	0·04
11‖	1·21	0·5	3·20	31	16·2	6·7	0·49	2·00	—	—	—	—	0·71	0·234	0·0252
12‖	1·21	0·5	3·20	120	65·7	27·0	2·0	2·00	—	—	—	—	0·105	3·65	0·394
13	1·21	2	3·40	31	8·20	3·23	0·23	1·75	4·40	2·23	1·27	1·80	0·90	0·11	0·012
14	1·21	2	3·40	120	67·0	26·0	1·89	1·90	3·75	3·36	0·48	1·88	0·043	3·50	0·38
15	1·21	2	3·20	31	8·11	3·4	0·25	1·00	—	—	—	—	0·93	0·119	0·0128
16	1·21	2	3·20	120	67·9	27·9	2·03	1·25	3·65	3·24	0·68	1·70	0·109	3·76	0·407
17_{AB}	1·21	4	2·98	31	8·35	3·7	0·27	1·25	—	—	—	—	1·02	0·129	0·0139
18_{AB}	1·21	4	2·98	120	67·3	29·7	2·2	1·50	3·70	3·29	0·64	3·42	1·123	4·0	0·43
19	1·21	2	2·87	31	35·3	16·2	1·2	2·00	4·05	2·57	1·20	1·61	0·71	0·57	0·061
20	1·21	2	2·87	120	35·3	16·2	1·2	1·875	3·75	3·02	0·83	1·97	0·22	2·19	0·236
21	1·21	2	1·02	31	10·51	13·6	1·0	2·00	4·10	2·57	1·24	1·65	0·75	0·47	0·051
22	1·21	2	1·02	120	10·51	13·6	1·0	1·875	3·75	2·90	0·95	1·95	0·36	1·83	0·198

23	1·21	2	1·02	31	45·5	59	4·3	1·875	4·00	2·88	1·12	2·02	0·47	2·06	0·221
24	1·21	2	1·02	120	45·0	58	4·2	1·875	3·95	3·58	0·41	2·16	0·02	7·8	0·847
25	1·21	2	0·17	31	8·07	62·6	4·5	1·875	3·95	2·84	1·12	1·69	0·47	2·2	0·215
26	1·21	2	0·17	120	5·56	43	3·0	1·75	3·80	3·40	0·56	1·92	0·063	5·80	0·63
27_{AB}	1·21	2	1·02	31	90·1	116	8·4	1·875	4·20	2·97	1·23	2·00	0·49	4·05	0·44
28	1·21	2	1·02	70	88·4	114	8·3	1·875	4·30	3·70	0·82	2·12	0·105	9·0	0·97
29	1·21	2	1·02	120	89·7	116	8·4	1·875	4·20	3·90	0·29	2·06	0·00	15·6	1·68
30	1·21	2	0·17	31	22·1	172	12·5	2·00	4·25	3·01	1·20	1·62	0·46	6·0	0·65
31	1·21	2	0·17	120	22·4	174	12·6	2·00	4·35	3·95	0·41	1·80	0·00	23·5	2·54
32	1·21	2	0·17	31	22·1	172	12·5	1·00	4·25	2·69	1·41	2·03	0·55	6·0	0·65
33	1·21	2	0·17	120	22·3	173	12·6	1·00	4·35	4·01	0·47	2·08	0·00	23·4	2·52
34	1·21	2	0·17	31	89·3	694	50·5	1·75	4·25	—	—	—	0·78	24·2	2·61
35	1·21	2	0·17	120	89·3	694	50·5	1·75	4·50	—	—	—	0·06	94	10·1
36‖	1·71	0·33	4·15	31	22·3	7·1	0·5	2·25	—	—	—	—	0·75	0·70	0·107
37‖	1·71	0·33	4·15	120	22·3	7·1	0·5	2·25	—	—	—	—	0·26	2·7	0·41
38	1·71	1	3·95	6	5·54	1·85	0·1	2·25	4·75	2·40	1·39	0·88	1·00	0·035	0·0054
39_{AB}	1·71	1	4·05	6	22·3	7·27	0·5	2·30	4·60	2·49	1·37	0·96	0·97	0·139	0·021
40	1·71	1	3·95	31	5·61	1·88	0·1	2·25	4·25	—	—	0·89	1·00	0·185	0·028
41	1·71	1	3·70	31	11·06	3·95	0·29	2·25	4·15	2·46	1·23	1·00	0·80	0·39	0·060
42_{ABCD}	1·71	1	4·04	31	22·2	7·3	0·5	2·25	3·90	2·49	1·14	1·04	0·68	0·719	0·110
43	1·71	1	3·80	31	43·7	15·2	1·1	2·25	3·65	2·63	0·99	1·04	0·45	1·50	0·23
44	1·71	1	3·80	120	11·02	3·84	0·28	2·25	3·65	2·63	0·99	1·04	0·45	1·45	0·224
45_{AB}	1·71	1	4·00	120	22·3	7·4	0·5	2·25	3·45	2·91	0·71	1·05	0·18	2·8	0·432
46	1·71	1	3·70	120	47·5	17·0	1·2	2·25	3·40	3·27	0·17	0·93	0·00	6·4	0·99
47	0·8 + 1·71	—	4·00	31	11·06	3·7	0·27	Superposition test, see table 2							
48	0·8 + 1·71	—	4·00	120	48·22	15·9	1·1	Superposition test, see table 2							

† The mean fluid velocity V_m was calculated from $V_m = 670/T$ (cm/sec) where T (sec) is the time of flow.

‡ The inlet length $\Lambda = 0{\cdot}13\,R\,\mathrm{Re}$.

§ The effective overall concentration C_{eff} was determined by integrating the measured particle passages through a cross-section. Where this was available it was used to determine the ratio $C(0, l)/C_{\mathrm{eff}}$. Otherwise C_0 was used in place of C_{eff}.

‖ Incomplete series performed for concentration checks.

TABLE 1. Summary of results

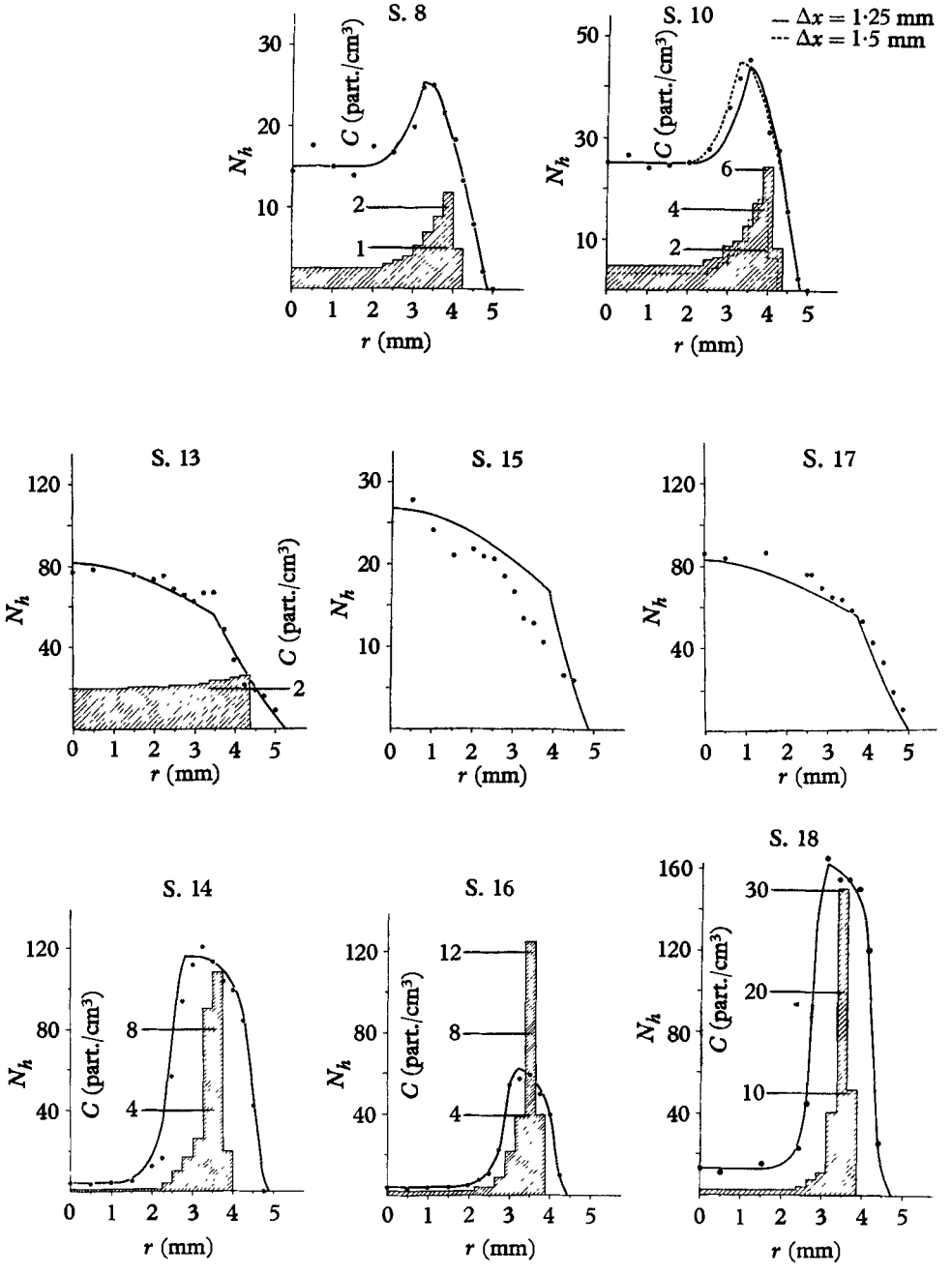

FIGURE 1. Distributions of 'hit' numbers N_h and concentration C with respect to radial position r. •, Experimental results for N_h. The histogram is the derived concentration distribution. The curve gives N_h reconstructed from histogram. For details on experimental conditions see table 1. *N.B.* The N_h-curves for S. 15 and S. 17 were derived from the concentration distribution of S. 13.

(*b*) *The development of the 'tubular pinch' effect*

As has already been shown in Part 1 the distributions measured are independent of the overall particle concentration. This shows that we are dealing with a single particle phenomenon and that the concentration changes are generated by dis-

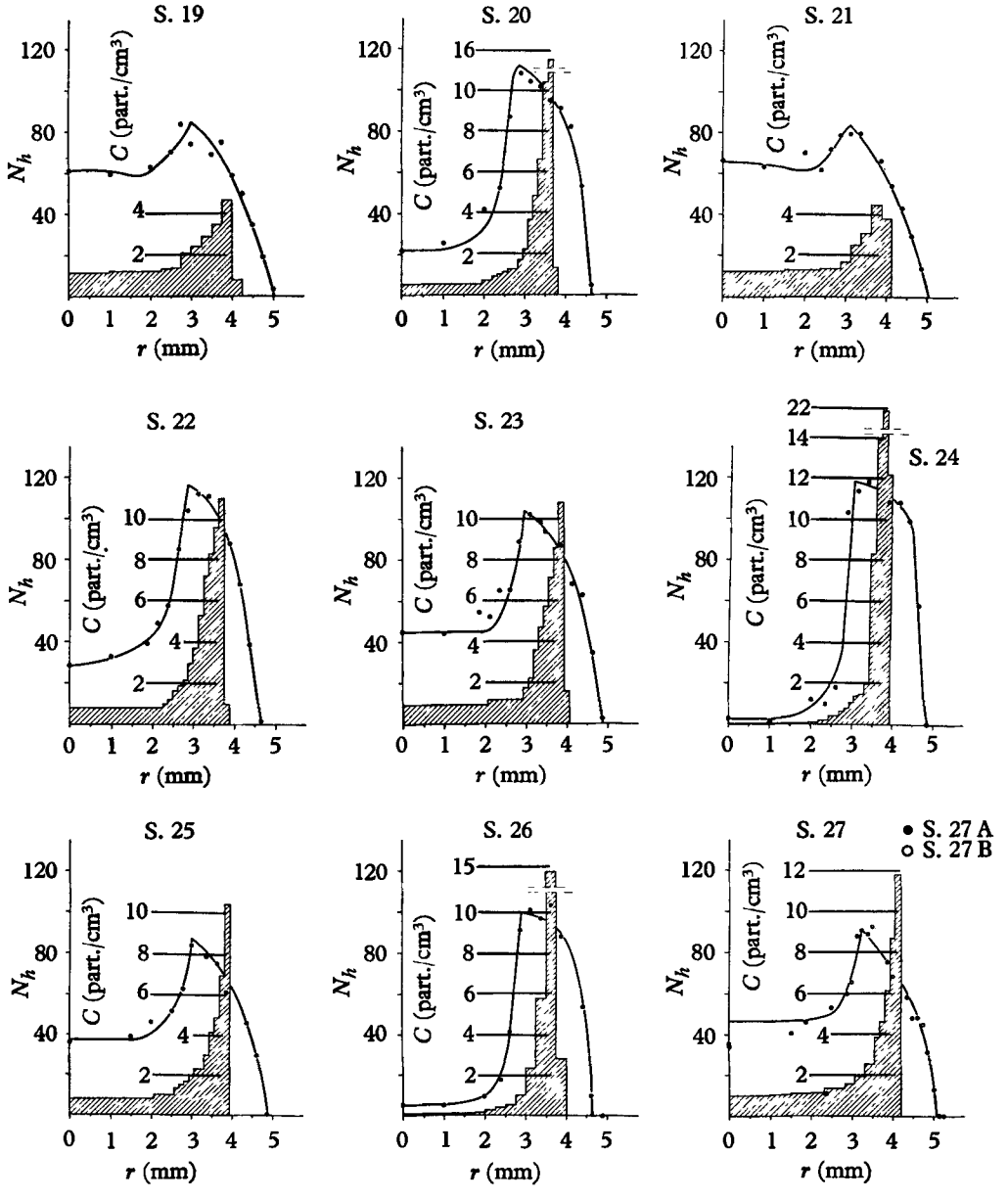

FIGURE 2. Distribution of 'hit' numbers N_h and concentration C with respect to radial position r. •, Experimental results for N_h. The histogram is the derived concentration distribution. The curve gives N_h reconstructed from histogram. For details on experimental conditions see table 1.

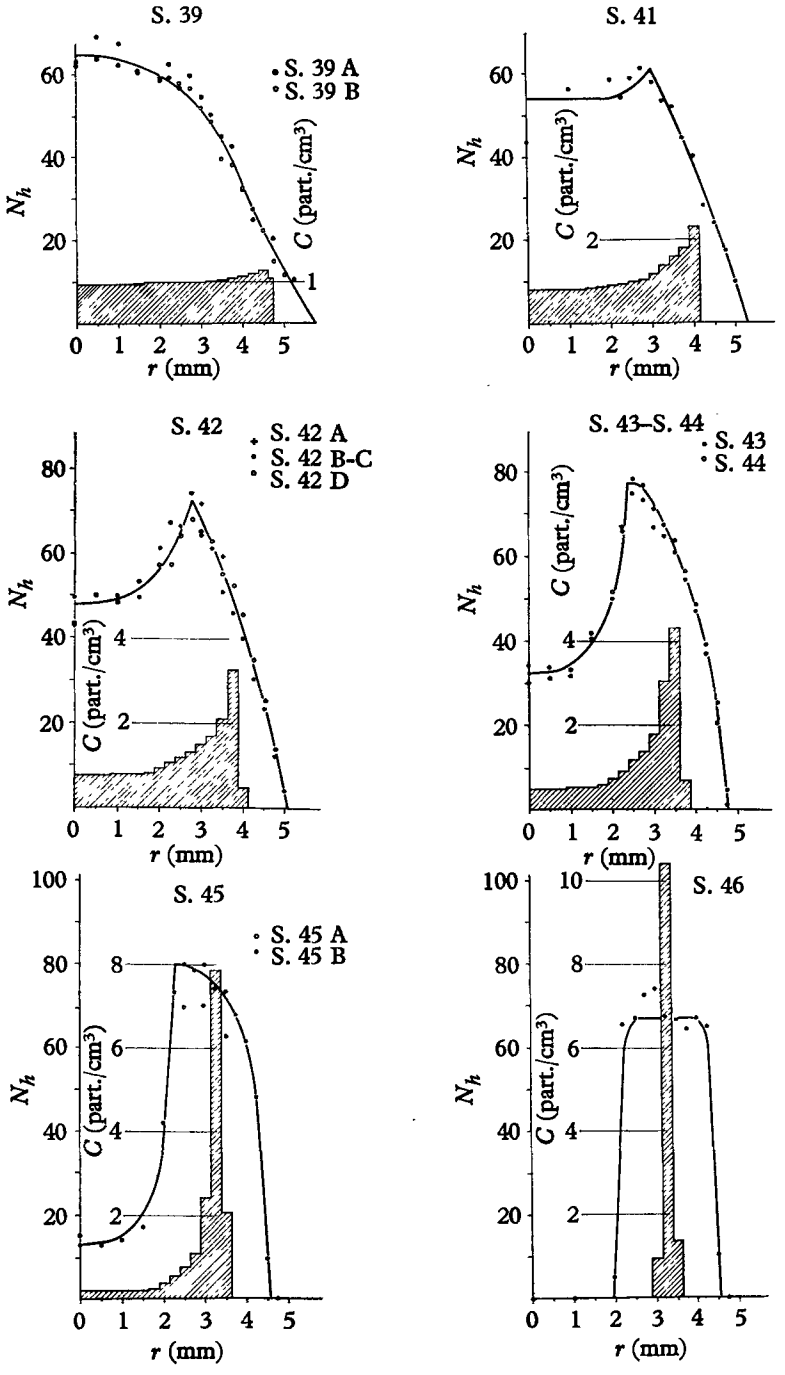

FIGURE 3. Same as figure 2.

placements whose size and direction are determined by the individual particle trajectory.

Detailed comparisons of results in cases where only the particle concentration was changed are possible and the series S. 8 and S. 10, as well as S. 14, S. 16 and S. 18, in figure 1, are examples of such cases. The ordinate scales for concentration C in these diagrams have been adjusted in the ratio of the overall concentrations so that direct superpositions of the histograms can be made.

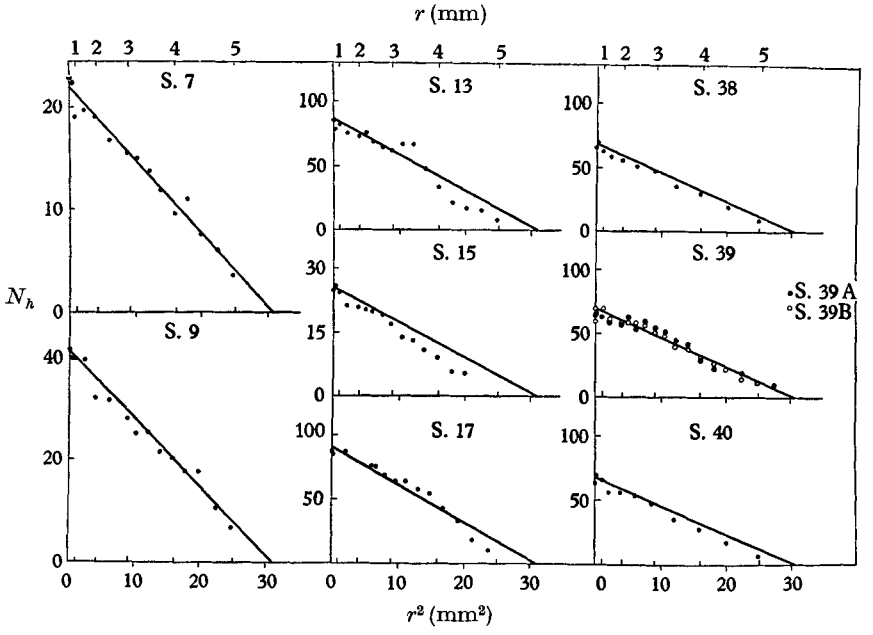

FIGURE 4. Plot of 'hit' numbers N_h against r^2. •, Experimental results for N_h. The lines are best-fit lines through theoretical intercepts on r^2-axis. For details of experimental conditions see table 1.

Another excellent illustration of the independence of particle movements was obtained when mixtures of particles of markedly different radii were studied. In table 2 we give the results of two such tests. The first two lines of data refer to cases of unmixed particles, series S. 9 and S. 10, corresponding to particles where $2a = 0{\cdot}8$ mm, and to series S. 41 and S. 46 corresponding to particles where $2a = 1{\cdot}71$ mm.

A mixture of 2 part./cm^3 of the smaller and 0·5 part./cm^3 of the larger size was then prepared and tested in series S. 47 and S. 48 under the same flow conditions as apply to the pair S. 9 and S. 41 and to the pair S. 10 and S. 46 respectively. A linear combination of the results for the unmixed systems, due allowance being made for different bulk concentration, agrees very well with the directly measured results. Note, moreover, that the distributions for the large and small particles differ considerably from each other. Particularly in the second superposition test the tubular pinch has almost completely developed in S. 46, while it is only barely visible in S. 10 (see figures 3 and 1).

This linear addition of effects shows, moreover, that the presence of particles

r (mm)	0	1	2	3	3·5	4	5
S. 9†	41·7	39·2	33·6	27·6	24·7	20·3	6·8
S. 41‡	43·5	56·5	58·5	58·0	52·0	40·0	9·8
Linear combination‖	63·5	67·4	62·8	56·6	50·7	40·3	11·7
S. 47§	58·0	63·0	65·5	57·6	52·5	38·0	12·0
S. 10†	25.0	24·0	25·0	36	45·5	31·0	0
S. 46‡	0	0	5·2	74	67·0	67·0	0
Linear combination‖	25·0	24·0	27·6	73	79·0	64·5	0
S. 48§	23·5	22·4	36·2	71	77·5	77·6	0

† Overall concentration of particles in this series: $C_0 = 2$ part./cm^3.
‡ Overall concentration of particles in this series: $C_0 = 1$ part./cm^3.
§ Overall concentration of particles in this series: 2 part./cm^3 of diameter 0·8 mm and 0·5 part./cm^3 of diameter 1·71 mm.
‖ Sum of N_h from the first line and $0{\cdot}5N_h$ from the second line.

TABLE 2. Number of 'hits' N_h as a function of radial position. (Superposition tests with a mixture of particles of 0·80 and 1·71 mm diameter.)

does not influence the average flow pattern of the fluid, and that this pattern maintains its character unchanged throughout our experiments.

The development of the effect can be seen from series S. 39, S. 42 and S. 45 in figure 3 which represent observations carried out at $l = 6$, 31 and 120 cm respectively under identical flow conditions. While the concentration is still practically uniform at $l = 6$ cm, almost all particles have already collected at the equilibrium position 114 cm further down. Other comparisons at different cross-sectional levels when the flow conditions were the same all lead to the same conclusion, as will be seen by selecting cases from table 1 and studying the corresponding histograms in figures 1 to 3. A measure of the development of the effect is also obtained by observing the outer radial position r_{11m} where the concentration goes to zero. We have listed the values of r_{11m} in table 1. It will be seen that r_{11m} rapidly approaches an asymptotic value.

It is, moreover, possible to confirm the essential character of the effect, i.e. the tendency of all particles to reach the same radial position, simply by observing the motion of the flowing particles at levels where the effect has developed completely. In these cases all particles are seen to move with practically identical velocity. For example, a direct analysis of the velocities of 30 particles chosen at random gave a dispersion about the mean of only 4 % and the mean velocity agreed well with that to be expected for particles situated at the equilibrium radial position as measured in the scanning experiments.

The gathering of all particles into a narrow annular region is also seen from observations in the collecting reservoir where in the absence of stirring a thin mantle of particles is observed to leave the tube and to follow the streamline pattern of the liquid.

(c) *Discussion of the particle trajectories*

(i) *General considerations.* In view of the stability of the laminar flow pattern in the tube it is logical to assume that the velocity v of the particle is a function of radial position only and that a unique trajectory exists which tends asymptoti-

cally to the radial position r^* at which the particles are seen to congregate. This implies that particles which enter the flow tube at an initial radial position r_0 travel along that part of the trajectory only which leads from r_0 to r^*. The trajectory is composed of two branches and a particle will travel along one or other of them depending on whether $r_0 < r^*$ or $r_0 > r^*$.

As already pointed out the z-component of the velocity is given by

$$v_z = dz/dt = V(r) = 2V_m[1-(r/R)^2], \tag{1}$$

and for the r component v_r we now write

$$v_r = dr/dt = U(r). \tag{2}$$

For reasons of symmetry it follows, moreover, that

$$U(0) = 0. \tag{3}$$

The slope of the trajectory in the (r,z)-plane is derived by dividing (1) by (2),

$$(dz/dr)_{\text{trajectory}} = V(r)/U(r). \tag{4}$$

As we are dealing with stationary flow, conservation of particles demands that

$$\operatorname{div} C\mathbf{v} = 0,$$

where $C = C(r,z)$ is the particle concentration measured at position (r,z), i.e.

$$\partial[rC(r,z)\,U(r)]/\partial r + \partial[rC(r,z)\,V(r)]/\partial z = 0. \tag{5}$$

From (5), in view of the definitions of U and V, we deduce that

$$rCU = \text{const.} \tag{6}$$

along the trajectory. Equation (6) may be used to calculate C from some initial distribution provided $U(r)$ is known.

If, on the other hand, we want to derive $U(r)$ from measurements of $C(r,z)$ this cannot be done on the basis of (6) as the trajectory is then not known. Instead we may use

$$U(r) = -\frac{1}{rC(r,z)}\int_0^r r'V(r')\frac{\partial C(r',z)}{\partial z}\,dr', \tag{7}$$

which is easily deduced from equation (5). Our experimental results for C as a function of z are, however, not sufficiently closely spaced for $\partial C/\partial z$ to be determined with any precision. A derivation of $U(r)$ using equation (7) will have to await more detailed experiments.

(ii) *The concentration gradient along the tube axis.* Information about the behaviour of $U(r)$ at small values of r is best derived from our data, using

$$\left(\frac{\partial \ln C}{\partial z}\right)_{r=0} = -\frac{2}{V(0)}\left(\frac{\partial U}{\partial r}\right)_{r=0} = \text{const.}, \tag{8}$$

which is based solely on equations (3), (5) and the independence of U and V from z. Plots of $\ln C$ at $r = 0$ against tube position z should thus be linear.

(iii) *Formal characterization of the radial velocity.* The radial velocity $U(r)$ may depend, in addition to r, on the mean velocity of flow V_m, the viscosity η, and

density ρ of the medium, the radius R of the tube, and the radius a of the particle. It is independent of z, as we have already pointed out. It may thus be represented by

$$U(r) = U(P) = V_m h(a/R, P, \mathrm{Re}), \tag{9}$$

where h is a function of the quantities a/R,

$$P = r/R, \tag{10}$$

and

$$\mathrm{Re} = (2\rho V_m R/\eta) \tag{11}$$

(the tube Reynolds number), which are dimensionless variables formed from the parameters on which U is assumed to depend.

From (8) we find

$$\left(\frac{\partial \ln C}{\partial z}\right)_{r=0} = -\frac{1}{R}\left[\frac{\partial h(a/R, P, \mathrm{Re})}{\partial P}\right]_{P=0} = \text{const.},$$

which, after integration, gives

$$\ln\left[\frac{C(0,z)}{C(0,z_0)}\right] = -\left[\frac{\partial h(a/R, P, \mathrm{Re})}{\partial P}\right]_{P=0} \frac{(z-z_0)}{R},$$

i.e.

$$\ln\left[\frac{C(0,l)}{C_0}\right] = -\left[\frac{\partial h(a/R, P, \mathrm{Re})}{\partial P}\right]_{P=0} \frac{l}{R}, \tag{12}$$

where the substitution $l = z - z_0$ has been made if z_0 marks the position of the mouth of the tube.

(iv) *Comparison with experiment.* In figure 5 we have plotted $\ln[C(0,l)/C_0]$ (taken from table 1) against the parameter $\mathrm{Re}\, l/R$. As is seen, the results for particle sizes $2a = 1{\cdot}21$ and $1{\cdot}71$ mm group well along two straight lines, indicating that we may rewrite (12) as

$$\ln[C(0,l)/C_0] = -g(a/R)\,\mathrm{Re}\, l/R \tag{13}$$

where, as shown, g is a function of (a/R) only.

We may conclude therefore that U, and with it also the radial force F, is linearly proportional to Re. The origin of the effect in the inertial components of the flow is demonstrated by its dependence on Re.

If we make the assumption that $g(a/R)$ is a power series in a/R whose leading term is of degree n and whose further terms may be neglected we may write

$$g(a/R) = \tfrac{1}{2}k_n[a/R]^n, \tag{14}$$

where k_n is a numerical constant. Using the slopes of the two full lines in figure 5 the power n defined above is found to be $n = 2{\cdot}84$. The dotted line in figure 5 is drawn for the case $2a = 0{\cdot}80$ mm when n has the value found above. The two data points available for these particles check rather well with this line.

The precision with which n can be determined depends greatly on the degree of monodispersity of the particle fractions. It can be shown that the error in n is proportional to the distribution width. In our case, where the smaller particles were less monodisperse than the larger ones, n may have been underestimated by about 10 %. [In our preliminary note (Segré & Silberberg 1961) a value of n of the

order 4 was reported, due to a faulty estimate of the diameter of the largest particles. This is 1·71 mm instead of 1·6 mm as there reported. The values of L there should be corrected for this change in figure 2 of that note.]

(v) *General characterization of distribution in reduced co-ordinates.* In order to discuss the behaviour at other radial positions we make the assumption that $\partial U(P)/\partial P$ may be expressed as a power series in P

$$\partial U(P)/\partial P = A_0 + A_1 P + A_2 P^2 + \ldots, \tag{15}$$

where

$$A_0 = [\partial U(P)/\partial P]_{P=0} = V_m \operatorname{Re} g(a/R), \tag{16}$$

as follows from equations (9), (12) and (13). Integration of (15) remembering (3) then leads to

$$U(P) = PV_m \operatorname{Re} g(a/R)\,(1 + B_1 P + B_2 P^2 + \ldots), \tag{17}$$

where $B_1 = A_1/2A_0$, $B_2 = A_2/3A_0$, etc., may in general be functions of the physical and geometrical parameters but are independent of r and z.

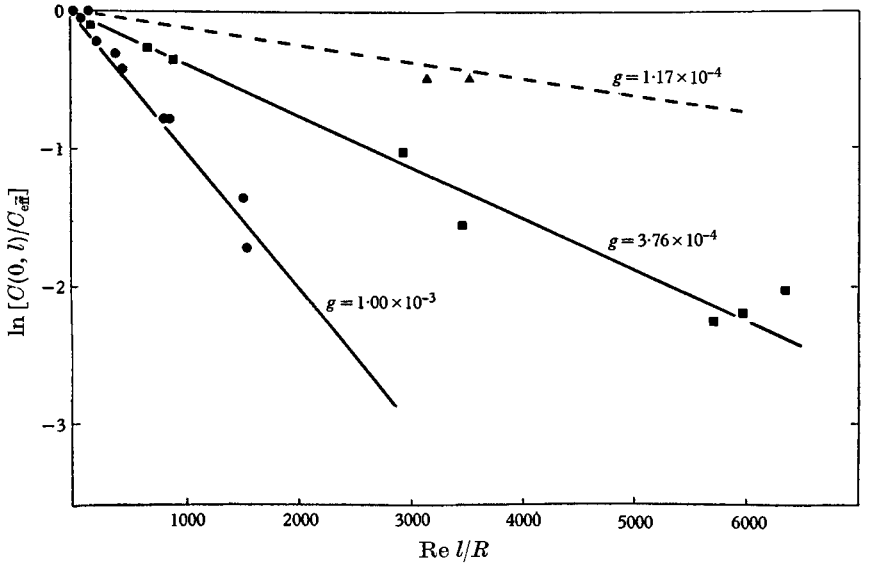

FIGURE 5. Plot of $\ln [C(0, l)/C_{\text{eff}}]$ against $\operatorname{Re} l/R$ for experiments at Reynolds numbers less than 30. Note grouping of experimental results into two straight lines for particle sizes $2a$ = 1·71 mm and $2a$ = 1·21 mm. Broken line drawn for particle size $2a$ = 0·80 mm is calculated on the basis of equation (14). ▲, $2a$ = 0·80; ■, $2a$ = 1·21; ●, $2a$ = 1·71.

The vanishing of the radial force at the position $P^* = r^*/R$ implies that the factor in square brackets in (17) has a root at that point whose value will be determined by parameters B_1, B_2, etc. Since P^* has been found to be constant within the experimental error in measurements performed over a wide range of Reynolds numbers and for different particle dimensions it may be concluded that the B's are numerical constants under these circumstances.

Substitution of (1) and (17) into (4) followed by integration from a position (P_0, z_0) at the tube mouth to a position (P_1, z) leads to the following expression

$$L_n = \frac{2}{k_n} \int_{P_0}^{P_1} \frac{(1-P^2)\,dP}{P(1 + B_1 P + B_2 P^2 + \ldots)}, \tag{18}$$

where $$L_n = l(\rho V_m/\eta)\,(a/R)^n \tag{19}$$

results from (14) and is a dimensionless measure of the distance l from the tube mouth. It follows from (18) that a particle setting out at the tube mouth from position P_0 will reach a uniquely defined position P_1 at a distance L_n down the tube.

The set of points P_0 marking the co-ordinates of the particles at the tube mouth thus goes over into a uniquely defined corresponding set of points P_1 at the

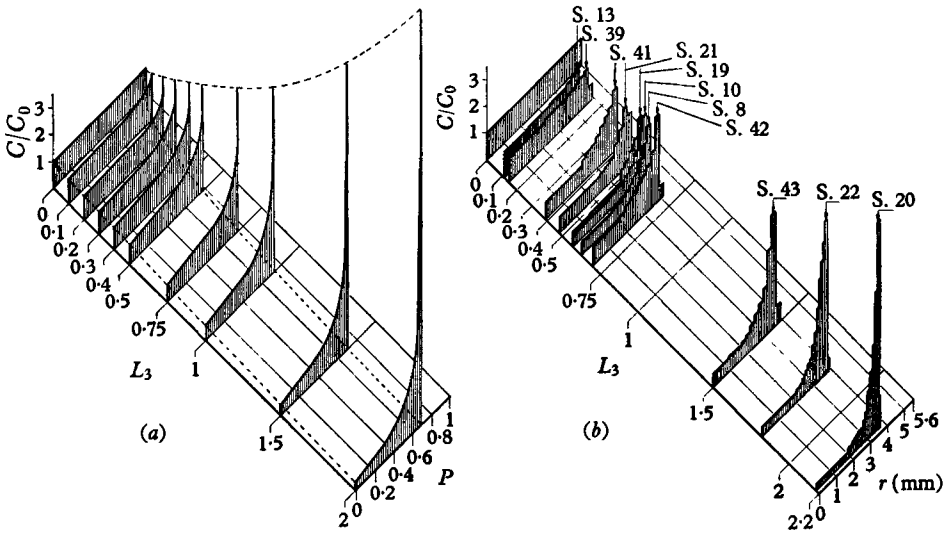

FIGURE 6. Concentration distribution in tube in reduced co-ordinates. (*a*) Theoretical model with quadratic force hypothesis. (*b*) Experimental results.

$$L_3 = \frac{\rho V_m l}{\eta}\left[\frac{a}{R}\right]^3 \qquad P = r/R.$$

level L_n. In other words, the given distribution of particle concentration at the tube mouth (uniform in our case) transforms into a uniquely defined distribution of concentration depending only on the choice of L_n. The distributions measured for series characterized by different experimental circumstances but by the same L_n-values should thus be identical.

The plot of figure 7 has shown that n is about 3. Taking into account the limited precision of this determination and assuming that n is integral we have calculated L_n for $n = 3$ and listed it in table 1. In addition, we have given the results for L_n in the case $n = 4$.

A three-dimensional array of the concentration distributions, for all series with Re < 30, in order of L_3 is shown in figure 6 (*b*). As can be seen the distributions fall into natural progressive order and clearly illustrate the development of the tubular pinch effect.

How exactly distributions superimpose may be seen from figure 3 where in the case of two series of practically the same L-value, S. 43 and S. 44, for which the Reynolds numbers are 15·2 and 3·8 respectively, the results are plotted on the same co-ordinates.

For the concentration distribution $C(r, z)$ we have calculated the positions $\bar{r}$ of the average of C along r

$$\bar{r} = \int_0^R rC\,dr \Big/ \int_0^R C\,dr,$$

and the second moment of this distribution about $\bar{r}$, i.e.

$$(\Delta r)^2 = \int_0^R (r-\bar{r})^2 C\,dr \Big/ \int_0^R C\,dr.$$

Both $\bar{r}$ and Δr are given in table 1 for all series and Δr is plotted against L_3 and L_4 in figure 7 for cases where Re < 30.

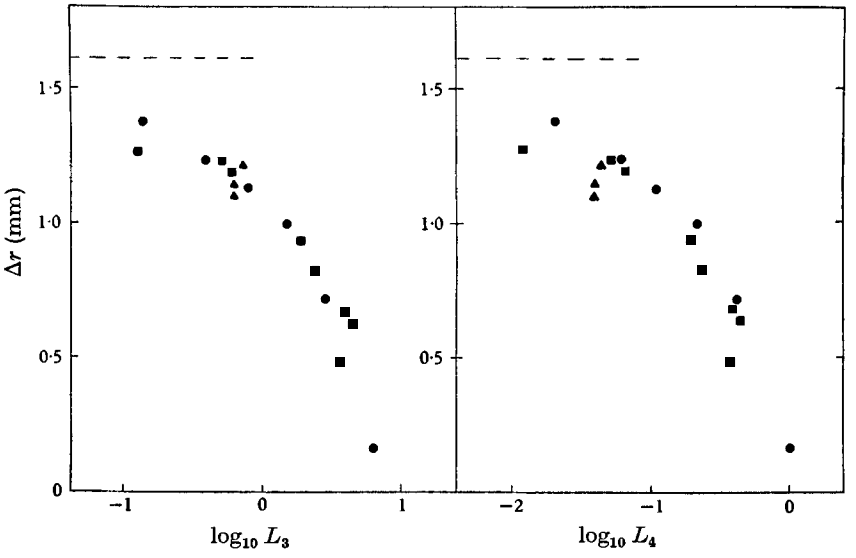

FIGURE 7. Concentration distribution parameters plotted against reduced tube lengths L_3 and L_4. ▲, $2a$ = 0·80 mm; ■, $2a$ = 1·21 mm; ●, $2a$ = 1·71 mm.

Note that the dotted line in figure 7 is the asymptotic level for Δr, as L_n tends to zero, on the asumption of a uniform concentration C_0 throughout the tube. If allowance is made for the fact that particles cannot approach the wall closer than their radius the level would be brought down by about 0·1 to 0·2 mm. As Δr characterizes the distributions in a sensitive and objective manner the high measure of correlation shown may be taken to confirm our basic assumptions. The evidence of figure 7 is also in favour of using $n = 3$ in (14).

It is obvious that the points r_{11m} already defined trace the outer branch of the trajectory. In figure 8 we show these points plotted against L_3. Note should be taken only of the full points as the others refer to high Reynolds numbers and will be discussed below. The full line corresponds to a theoretical model and neglects the restriction of finite particle dimensions at the tube wall. The deviations from this line at low L-values are due to that. Among themselves the points correlate well in these co-ordinates, but in this case the correlation would even be improved if plotted against L_4.

(d) Deviation at larger Reynolds number

When experiments were performed at larger Reynolds numbers, deviations from the above picture were observed. The general tendency was to blur the sharpness of the tubular pinch, i.e. to increase the spread Δr of the distribution, to decrease the width of the particle-free region near the wall, i.e. to increase the value of r_{lim} which marks this position, and to cause the concentration at the centre to

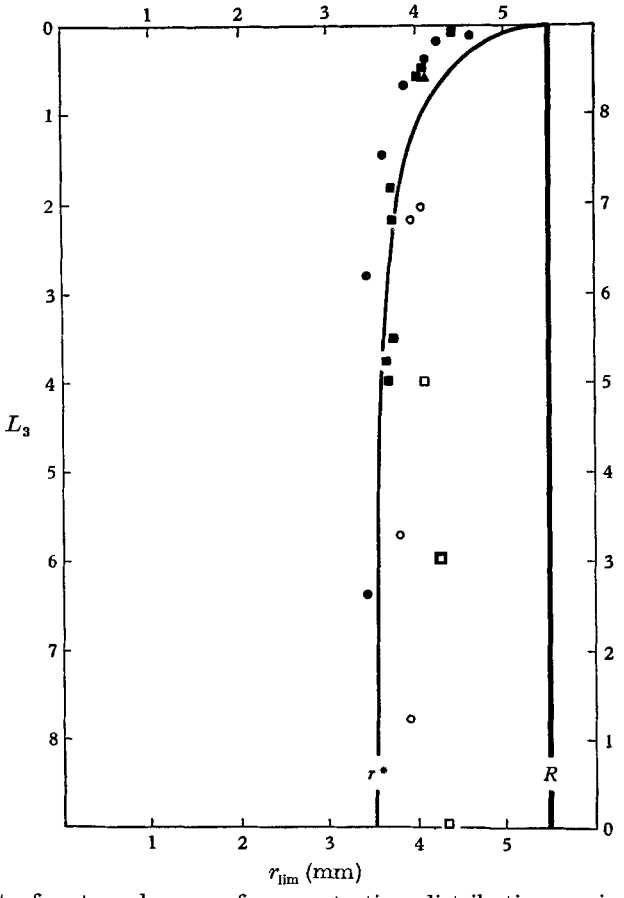

FIGURE 8. Plot of outer edge r_{lim} of concentration distribution against reduced tube length L_3. The points are experimental results. The curve is derived from the quadratic force model. ▲, $2a$ = 0·80, Re < 30; ■, $2a$ = 1·21, Re < 30; ●, $2a$ = 1·71, Re < 30; ○, 30 < Re < 100; □, 100 < Re. a is in mm.

decrease more slowly than expected from equation (13) (see table 1 and figure 8, open points). Whereas the points at Reynolds numbers below 30 fall well within the consistency framework established in the previous section, results obtained at high Reynolds numbers deviate from this picture in systematic fashion beyond the possibility of experimental error.

Although the Reynolds numbers cited are relatively large, laminar flow patterns would still be expected in most cases, at any rate for the particle-free liquid. To what extent any turbulence which enters the mouth of the tube is carried along

and to what extent the presence of particles may cause disturbance is hard to evaluate. Moreover the inlet length Λ in some cases approaches or even exceeds the l-value.

On the other hand, a 'tubular pinch' does develop, at least qualitatively, and only at really large Reynolds numbers when turbulence is surely present is the effect almost completely blurred out (as in the case for series S. 1–S. 6, S. 34 and S. 35).

The origin of these deviations even under laminar conditions are not hard to understand. First of all the force F is a power series in Re. This means that the B's in equation (17) will depend on Re when Re is large enough and that the solution r^* for the equilibrium position becomes a function of Re, as is indeed observed.

On the other hand the general solution of the problem remains expressible as a function of the non-dimensional combinations Re, a/R and l/R so that the same distribution should arise for given a/R and l/R in whatsoever a manner a given value of the Reynolds number is obtained (by a different choice of velocity and viscosity). An illustration of this is provided by series S. 23 and S. 25 in figure 2.

(*e*) *Effects at higher concentrations*

As already pointed out in Part 1 a concentration dependence of the results may be expected to appear at concentrations not much above those employed. This is particularly true for those situations where the tubular pinch has built up high local concentrations. That inter-particle interactions occur in these cases is shown by the observation that groups of particles moving at the position of the peak generally tend to arrange themselves into linear, regularly spaced rows in the direction of flow. The gap between particles in these rows is equal to about one particle diameter. The build up of these 'necklaces' has been followed visually and clear cases of 'capture' of spheres at the ends of the rows were observed. Often two necklaces which are sufficiently close to each other rearrange themselves into one large linear array. If the end particles are not initially at their proper distance apart they have been observed to rock themselves into the appropriate equilibrium position.

Where particles moving along colliding paths come into contact the dumbbell formation described by Manley & Mason (1952) could sometimes be observed.

These phenomena are here described for their intrinsic interest but were not followed up systematically.

5. Theoretical implications of results

The possibility of representing our results uniquely in a framework of reduced co-ordinates L_n and P may be taken as justification for the basic assumptions underlying our derivation of these variables. These assumptions were, primarily, the origin of the radial force in the inertia of the fluid and the independence of the particle velocity of position along the tube axis. The occurrence of the 'tubular pinch' at a fixed value $P^* = 0{\cdot}63$ confirms, moreover, that the coefficients B in (17) are numerical constants which are not all zero.

If we consider as the simplest model, compatible with these conclusions, the case

$$B_i = 0 \quad (i \geqslant 2), \qquad B_1 = -1/P^*,$$

we can introduce (17) into (6) and determine the values of C along the trajectory. Equation (18) thus enables the concentration profile to be plotted for any given value of L_n. In figure 6 (a) we show the results of such a calculation and note that they compare well with the experimental profiles given in figure 6 (b). A quadratic dependence of the force on radial position is thus shown to be a reasonable working hypothesis.

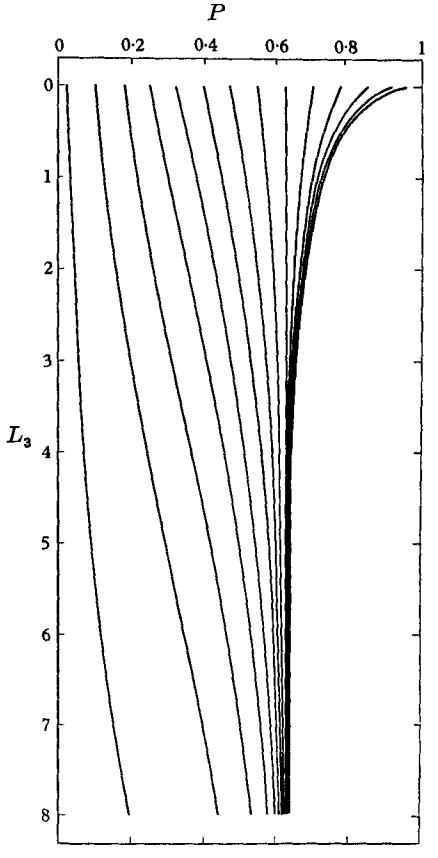

FIGURE 9. Trajectories for quadratic force model in reduced tube co-ordinates.

Figure 9 gives a plot of the trajectories originating at different initial radial positions in the case of this model. The extreme trajectory is plotted also in figure 8 for comparison with the experimental r_{lim} values.

At higher Reynolds numbers, this model breaks down as already pointed out. Note, moreover, that an increase in a/R must also eventually bring about deviations in behaviour. The two a/R values from which practically all the comparisons arise are obviously insufficient to establish the functional dependence on particle dimensions. In fact, if we are already examining a region where deviations of the type discussed above may play a role, the assumption (14) would be inadequate and the precise meaning of the n-value derived would be in doubt.

Theoretical reasons according to which n should be 4 will now be given. If we follow Tollert (1954) and attribute the effect to a Magnus force and use the Kutta–Joukowsky formula, or if we take the result of Rubinow & Keller (1961) for a spinning sphere in a viscous fluid we are led to an expression in which the force is proportional to the vector product of the relative velocity $\mathbf{v}_{\text{rel.}}$ of sphere and fluid and the angular velocity Ω of the spheres.

For these magnitudes we can turn to the solutions found by Simha (1936) in his creeping-motion approximation already quoted:

$$|\Omega| = 2V_m r/R^2, \tag{20}$$

and

$$|\mathbf{v}_{\text{rel.}}| = \tfrac{4}{3}V_m(a/R)^2. \tag{21}$$

If we approximate the sphere by a cylinder of length $2a$ in the Kutta–Joukowsky formula and introduce the Simha velocities we find

$$F(r) = k_{K-J}[V_m^2\rho a^5/R^4]r, \tag{22}$$

where k_{K-J} is a numerical constant. The use of the Rubinow & Keller expression leads to the same result but the numerical constant k_{R-K} is different.

k_{K-J}	k_{R-K}	k_S	$6\pi k_4$
−33·5	−8·4	−64·3	87

TABLE 3. Numerical constant in radial force expression

Also the treatment of Saffman (1956) gives an expression for the force of the above type but with still another numerical constant k_S. We have listed the values of these constants in table 3. On the other hand, use of the Stokes resistance formula and equations (14) and (17) gives

$$F(r) = 6\pi k_n[V_m^2\rho a^{n+1}/R^n]r[1 + B_1(r/R) + \ldots]. \tag{23}$$

It is clear therefore that the theoretical deductions can be made to agree with the leading term in equation (23), as far as functional dependence on a is concerned, when putting $n = 4$. Note, however, that while k_{K-J}, k_{R-K} and k_S are all negative $6\pi k_4$ is positive. The existence of the 'tubular pinch' effect thus demands a force opposite in direction to the theoretical expectations in the central region of the tube.

Unfortunately none of the treatments leading to the result (22) are exactly applicable to the circumstances of our case. The Kutta–Joukowsky formula has been derived in two dimensions for the potential flow of an ideal liquid in steady motion past a rotating infinite cylinder, and while the Rubinow & Keller treatment considers the case, closer to ours, of a spinning sphere in a viscous fluid in steady flow the introduction of the Simha velocities into either of these expressions in justifiable only on very formal grounds. Saffman, by a method of successive iteration, approximates the solution of the Navier–Stokes equations for the case of a sphere carried along in an infinite Poiseuille field of flow. His treatment is thus an extension of the Simha solution and may be regarded as most closely

comparable with our case. The absence of walls in his treatment and possible doubts about the convergence of the method may be seen as the only sources for the discrepancy in the value and sign of the numerical constant. On the other hand, the functional dependence on the physical and geometrical parameters of the leading term in Saffman's result is not likely to change by improvements in the calculation.

An explanation of why the exponent n does not turn out to be 4 thus has to take account of the walls and the reaction which the particle experiences in their presence. It is known, for instance, from treatments based on the linearized Navier–Stokes equations, that the drag on spherical particles moving parallel to a rigid wall deviates from the Stokes resistance by a term linear in particle radius (Happel & Brenner 1958). If the effective relative velocity between particle and liquid were increased by such an additional term its magnitude would be proprotional to a and not to a^2 as in the Simha slip velocity, equation (21). The use of such a relative velocity in the Rubinow & Keller expression, for example, would lead to an equation for the transverse velocity proportional in its leading term to the third rather than the fourth power of (a/R). The sign of the radial velocity would however be left unchanged. The presence of the walls is anyhow a cardinal feature of this system and no treatment which does not explicitly consider inertia effects in their presence can hope to be adequate.

A further insight into the nature of the effect may perhaps be obtained, experimentally, by adding a constant relative velocity component to the particle in the z-direction, an effect which could be realized by a density difference between particle and fluid causing a steady rate of sedimentation in the vertically placed flow tube.

Our results pose an interesting question about the applicability of the criterion of minimum energy dissipation which many authors following Jeffery (1922) regard as determining the sign of the radial force. The distribution arrived at in our case clearly contravenes this criterion.

The high dependence of the effects on particle dimension makes it worth while to examine the possibility of exploiting the phenomenon for the fractionation of mixtures. It is interesting that such an idea has been applied recently by Steenberg & Wahren (1960) to separate fibre fines from pulp suspensions.

It should be stressed, however, that the effect was established only for rigid spherical particles at relatively low concentration. The features which characterize the behaviour of concentrated suspensions of non-spherical, deformable particles, as in the case of fibres and of blood, may not necessarily follow from the observations here recorded. Furthermore, cases where Brownian motion could play a role are of course excluded from these considerations.

Thanks are expressed to Cartiera Vita Mayer and Co., Milan, who supported the extensive stay of one of us (G. S.) at the Weizmann Institute of Science.

REFERENCES

BAYLISS, I. E. 1960 *Flow Properties of Blood.* Oxford: Pergamon Press.

FREY-WYSSLING, A. 1952 *Deformation and Flow in Biological Systems.* Amsterdam: North Holland Publ. Co.

GOLDSMITH, H. L. & MASON, S. G. 1961 *Nature, Lond.*, **190**, 1095.

HAPPEL, J. & BRENNER, H. 1958 *J. Fluid Mech.* **4**, 195.

JEFFERY, G. B. 1922 *Proc. Roy. Soc.* A, **102**, 161.

LORENTZ, H. A. 1907 *Abhandlungen über Theoretische Physik.* Leipzig.

MANLEY, R. ST. J. & MASON, S. G. 1952 *J. Coll. Sci.* **7**, 354.

MAUDE, A. D. & WHITMORE, R. L. 1956 *Brit. J. Appl. Phys.* **7**, 98.

POISEUILLE, J. L. M. 1836 *Ann. Sci. Nat.* (2), **5**, 111.

RUBINOW, S. I. & KELLER, J. B. 1961 *J. Fluid Mech.* **11**, 447.

SAFFMAN, P. G. 1956 *J. Fluid Mech.* **1**, 540.

SCOTT-BLAIR, W. G. 1958 *Rheologica Acta*, **1**, 123.

SEGRÉ, G. & SILBERBERG, A. 1961 *Nature, Lond.*, **189**, 209.

SEGRÉ, G. & SILBERBERG, A. 1962 *J. Fluid Mech.* **14**, 115.

SIMHA, R. 1936 *Kolloid Z.* **76**, 16.

SMITH, A. M. O. 1960 *J. Fluid Mech.* **7**, 565.

STEENBERG, B. & WAHREN, D. 1960 *Svensk Papperstidning*, **63**, 347.

TAYLOR, M. 1955 *Aust. J. Exp. Biol.* **33**, 1.

TOLLERT, H. 1954 *Chem. Ing. Tech.* **26**, 141, 270.

VAND, V. 1948 *J. Phys. Chem.* **52**, 300.

VEJLENS, G. 1938 *Acta Path. Microbiol. Scand.* (Suppl.), no. 33.